Stem Cell Research & Therapy

RESEARCH

Open Access

hUMSC-derived exosomes alleviate follicular interstitial cell autophagy by let-7a-5p/AMPK/mTOR axis in POI rats

Yu Tang[1,2†], Yu He[1†], Xingyu Huo[1], Juntong Chen[1], Maojiao Qian[1], Haoyu Huang[1], Yixuan Meng[1], Lianshuang Zhang[1], Feibo Xu[1], Yukun Zhang[1], Hongchu Bao[3,4*] and Yanlian Xiong[1*]

Abstract

Background One major factor contributing to infertility in women of childbearing age is premature ovarian insufficiency (POI). Exosomes produced from human umbilical cord mesenchymal stem cells (hUMSC-Exos) have drawn a lot of attention lately as a potential treatment for ovarian dysfunction brought on by POI. However, its therapeutic mechanism is still unclear and needs further exploration.

Methods POI model was established by intraperitoneal injection of cyclophosphamide (CTX) in female Wistar rats. These POI rats were treated with hUMSC-Exos for one week. In addition to in vivo experiments, in vitro POI models were also established. In vitro experiments, theca interstitial cells (TICs) treated with CTX were exposed to normal as well as let-7a-5p inhibitory hUMSC-Exos. The ovary structure, morphology, endocrine function, and reproductive ability of POI rats were observed by H&E staining and ELISA. Western blot, immunofluorescence staining (IF), and quantitative real-time polymerase chain reaction (qRT-PCR) were used to evaluate the autophagy-related indexes in ovary and TICs of POI rats in each group.

Results CTX induced abnormalities of ovarian morphology, structure, endocrine, and reproductive function in rats, and accompanied by autophagy of TICs. Notably, hUMSC-Exos diminishes ovarian structural and functional damage in POI rats and TICs autophagy via targeting the AMPK/mTOR pathway. Furthermore, downregulating let-7a-5p in hUMSC-Exos weakened their ability to prevent TICs autophagy.

Conclusions Overall, the findings suggested that hUMSC-Exos improves ovarian function in POI rats by inhibiting TICs autophagy via the let-7a-5p/AMPK/mTOR pathway. Our study provided further evidence that POI patients can benefit from hUMSC-Exos-mediated therapy.

Keywords POI, hUMSC-Exos, Theca interstitial cells, let-7a-5p, Autophagy

†Yu Tang and Yu He contributed equally to this work.

*Correspondence:
Hongchu Bao
baohongchu@163.com
Yanlian Xiong
xyl8807@163.com

[1]Xu Rongxiang Regenerative Medicine Research Center, School of Basic Medicine, Binzhou Medical University, Yantai, P.R. China
[2]Department of Physiology, School of Medicine, Shandong College of Traditional Chinese Medicine, Yantai, P.R. China
[3]Reproductive Medicine Centre, The Affiliated Yantai Yuhuangding Hospital of Qingdao University, Yantai, China
[4]Shandong Provincial Key Medical and Health Laboratory of Reproductive Health and Genetics, Yantai Yuhuangding Hospital, Yantai, China

Introduction

Premature ovarian insufficiency (POI) is a disorder that causes ovarian malfunction. Symptoms of this disease include infrequent or missing menstruation, infertility, and menopause [1]. Recently, research has revealed that damage to theca interstitial cells (TICs) is a major cause of POI [2, 3]. Mesenchymal stem cells (MSCs) have attracted a lot of attention as a potential treatment for POI. Our most recent work also discovered that human umbilical cord mesenchymal stem cells (hUMSCs) regulate TICs autophagy and restore ovarian function [4]. However, the exact process by which hUMSCs regulate TICs requires additional investigation.

POI, a major cause of infertility in women of reproductive age, is defined by a reduction in serum estradiol (E_2) and anti-Mullerian hormone (AMH) levels and an increase in gonadotropin levels [5]. Research has demonstrated that chemotherapy drugs such as cyclophosphamide (CTX) disrupt immune regulation, cell viability, promote inflammation, and lead to ovarian microenvironment imbalance, ultimately inducing POI [6, 7]. Furthermore, investigations have found that POI is also accompanied by ovarian tissue fibrosis, oxidative stress, and cell death [8, 9]. Recently, Dou et al. determined that granulosa cells (GCs) autophagy triggered by the Phosphatidylinositol 3-kinase (PI3K)/protein kinase B (AKT)/Mammalian target of rapamycin (mTOR) signaling pathway is a plausible biological mechanism for causing POI [10]. Autophagy is the process by which cells digest and recycle proteins and organelles to maintain intracellular balance [11]. In general, autophagy protects cells, nevertheless, interruption of autophagy pathways or excessive autophagic flux usually results in cell death [12]. Our latest research has also revealed that TICs, the important cells that control follicle formation and hormone synthesis, also suffer from autophagy disorders mediated by the AMPK/mTOR pathway during POI [4]. However, the particular mechanism and associated treatment approaches to autophagy have not been investigated.

Exosomes, a subset of extracellular vesicles (EVs), function as a mode of molecular transfer and intercellular communication, and enable direct extracellular transfer of lipids, RNA/DNA, and cytokines between cells. MSC exosomes have recently drawn interest as a potential treatment for a number of aging-related illnesses [13]. Yang and colleagues found that human mesenchymal stem cell-derived exosomes (hUMSC-Exos) improved the senescence of GCs, which relieved POI [14]. Qu et al. found that hUMSC-Exos promoted ovarian angiogenesis and reinstated ovarian function in POI rats [15]. Furthermore, a plethora of studies suggest that stem cell exosomes influence tissue cell metabolism, differentiation, and apoptosis by controlling the autophagy pathway [16]. Ren and colleagues discovered that adipose-derived stem cell-derived exosomes (ADSC-Exos) minimize POI by inhibiting GCs apoptosis and autophagy [17]. Nevertheless, the potential molecular processes by which MSC-Exos regulate the autophagy pathway of crucial cellular components in ovarian tissue, such as TICs and GCs, subsequently affect cellular metabolism and function during the POI process have yet to be fully understood.

Thus, our goal in this work was to investigate the molecular mechanism by which hUMSC-Exos regulates TICs metabolism, particularly the autophagy pathway, thereby clinically alleviating ovarian structural and functional abnormalities during POI.

Materials and methods

Reagents

DAPI (#BD5010) and antibodies against AMPK (#BS40316), Beclin (#MB0030) were obtained from Bioworld corporation (Dallas, Texas, USA). mTOR (#2983S), p-mTOR (#5536S) were obtained from CST corporation(Massachusetts, USA). LC3 (#14060-1-AP), p62 (#66184-1-1 g), GAPDH (#10494-1-AP), RP-conjugated secondary antibodies (#SA00001-2) were obtained from Proteintech corporation (Chicago, Illinois, USA). p-AMPK (#B29A008) was obtained from Absin Corporation (Shanghai, China). Cyp17a1 (#EPR6294), and FSHR (#ab75200) were obtained from Abcam Corporation (Cambridge, MA, USA). Enhanced chemiluminescence reagent (ECL) (#Tc-PE0010) kits were obtained from Biosharp Corporation (Hefei, China).

Animals

Seven-week-old female Wistar rats were purchased from Jinan Pengyue Experimental Animal Breeding Co., Ltd. for in vivo experiments. The weight of these rats ranged from 190 to 210 g. All animals were housed in facilities with suitable temperature and humidity, with free access to drinking water and rat chow. To minimize pain, the rats were anesthetized with pentobarbital sodium (200 mg/kg, i.p.) and sacrificed by cervical dislocation at the end of the experiment. Rats were confirmed dead when there was no autonomous respiration and no reflex activity, and no heart activity.

Establishment of POI model and groups

After one week of acclimatization feeding, Wistar rats were randomly divided into four groups ($n = 20$/group): control group, POI group, PBS group, and hUMSC-Exos group. The control group received intraperitoneal injections of 200 μL phosphate-buffered saline (PBS) containing 0.01% dimethyl sulfoxide (DMSO) from days 1 to 14. CTX was dissolved in 0.01% DMSO and injected intraperitoneally to establish the POI model, with a dosage of 50 mg/kg on day 1, followed by daily injections of 8 mg/kg from days 2 to 14. On days 15 and 18, rats in the PBS

group received 300 μL PBS via tail vein injection, while rats in the hUMSC-Exos group received 300 μL of PBS containing 150 μg hUMSC-Exos. Care was taken to avoid rapid injection to prevent congestive heart failure. On day 26, five rats from each group were randomly selected for fertility testing. The remaining rats were weighed and recorded, and ovaries and serum were collected to measure and record the wet weight of ovarian tissue. The experimental protocol was approved by the Animal Ethics Committee of Binzhou Medical University (Approval No: 2023-24). The work has been reported in line with the ARRIVE guidelines 2.0.

Extraction and identification of hUMSC-Exos

hUMSCs were collected from the umbilical cords of healthy neonates. The isolation, culture, and characterization of hUMSCs were conducted according to our laboratory's previous studies [18]. For the extraction of hUMSC-Exos, as described previously [19], the supernatant was collected when the 3rd to 5th generation of hUMSCs reached 80% confluence in culture dishes. Briefly, the collected supernatant was centrifuged at 200×g for 30 min at 4 °C. It was then mixed overnight with VEX exosome separation reagent (Vazyme, China) at 4 °C. The supernatant was collected again and centrifuged at 10,000×g for 1 h, with the pellet resuspended in PBS and kept at low temperature or used immediately. The isolated exosomes were identified using transmission electron microscopy (TEM) (JEOL JEM-1230, Tokyo, Japan), western blot of exosomal surface marker proteins (CD63, CD9, and HSP70, and use Cytochrome-C (Cyt-c) as a negative control), and NanoSight analysis (Malvern Instruments, Malvern, UK).

TICs culture and Co-culture with hUMSC-Exos

Using a method proposed in our previous study, TICs were isolated from the ovarian tissue of 4-week-old Wistar rats [20]. TICs were cultured in McCoy 5 A medium containing 10% fetal bovine serum (AusGeneX, Australia) and 1% penicillin and streptomycin (Corning, USA). The cells were maintained in an incubator at 37°C with 5% CO_2, with daily observations of growth status and passaging approximately every 3 days.

To knockdown and overexpression let-7a-5p in hUMSCs and TICs, inhibitor NC, let-7a-5p inhibitor, mimic NC and let-7a-5p mimic (Ribobio, China) were used to treat the hUMSCs and TICs. Subsequently, collect and purify hUMSC-Exos. The sequences were as follows: inhibitor NC, 5'- UUGUACUACACAAAAGUACUG-3'; let-7a-5p inhibitor, 5'- AACUAUACAACCUACUACCUCA-3'; mimic NC, 5'-UUCUCCGAACGUGUCACGUTT-3' and let-7a-5p mimic, 5'- UGAGGUAGUAGGUUGUAUAGUU-3'. 10 μg/ml of hUMSC-Exos was added to TICs and cultured at 37 °C with 5% CO_2 for 48 h. The purified hUMSC-Exos were incubated with 1,1'-dioctadecyl-3,3,3',3'-tetramethylindocarbocyanine perchlorate (Dil; Bioesn, China) at 37 °C for 60 min. After incubation, hUMSC-Exos were centrifuged at 1500 rpm for 5 min. Dil-labeled hUMSC-Exos were resuspended in PBS and incubated with TICs at 37 °C for 1 h. Finally, the nuclei were counterstained with DAPI, and fluorescence images were captured using an inverted fluorescence microscope (Leica, Germany).

Tracking Dil-labeled hUMSC-Exos

To evaluate the distribution of hUMSC-Exos in the ovaries of rats, 300 μl of PBS containing 1000 μg of hUMSC-Exos was injected via the tail vein into Wistar rats. The control group received an injection of 300 μl of PBS. After 48 h, abdominal and lateral imaging was performed using the IVIS Lumina III system (PerkinElmer, UK).

Observation of the estrous cycle

The estrous cycle of Wistar rats was observed at 8:00 am. First, a sterilized cotton swab, soaked in 0.9% NaCl solution, was gently inserted into the rat's vaginal tract and quickly and gently rotated counterclockwise. The swab was then smeared onto a dry carrier slide to obtain a smear of the rat's vaginal tract exfoliated cell smears. The smear was stained with St. Regis compound staining solution (Baso, China) and rinsed for about 8 min before being allowed to air dry. Finally, the cell morphology and staining were observed using an optical microscope (Echo, USA).

Hematoxylin-eosin staining (H&E)

Ovarian tissues from each group were fixed in 4% paraformaldehyde for 24 h. They were then embedded in paraffin, sectioned, baked, and deparaffinized before being immersed in water for H&E staining. Ovarian morphology was observed using an optical microscope, and the number of ovaries and follicles was assessed blindly using a histological scoring system from previous studies [20].

Enzyme-linked immunosorbent assay (ELISA)

Serum from each group of rats was collected to measure the levels of E_2, AMH, follicle-stimulating hormone (FSH), and luteinizing hormone (LH) using ELISA kits (Enzyme-linked Biotechnology, China). Additionally, the supernatant from TICs was also analyzed for E_2 and testosterone (T) levels using ELISA kits.

MiRNA library construction and sequencing

miRNA was extracted from hUMSC-Exos using the RNeasy Plus Mini Kit (QIAGEN, Germany). For small RNA library generation, 50 ng of exosomal RNA was used for each sample. Small RNA sequencing was

performed using the HiSeq 2500 (Illumina, USA), with read lengths ranging from 15 to 41 bp.

Quantitative real-time polymerase chain reaction (qRT-PCR)

Real-time PCR was used to detect the expression of miRNA and mRNA. Data from at least three replicates were calculated using the $2^{-\triangle\triangle CT}$ method. U6 served as the internal control for let-7a-5p, while GAPDH was the internal control for mRNA. Primer information is provided in Additional file 1.

Data acquisition and processing

We downloaded the transcriptome dataset for the mouse POI model (GSE 217193) from GEO, which includes three samples of normal ovarian tissue and three samples of POI ovarian tissue. Autophagy-related genes were obtained from the GeneCard website, and genes with a score of 4 or higher were selected to construct the autophagy pathway gene set.

BP, MF, KEGG pathway, CC analysis

Biological process (BP), molecular function (MF), Kyoto Encyclopedia of Genes and Genomes (KEGG) pathway, and cellular component (CC) enrichment analyses of the target genes of let-7a-5p were conducted using Metascape and DAVID software. The differential gene analysis of GEO data was conducted using the "limma" R package (version 3.42.2), with the criteria set as|logFC|>0.5 and P.val<0.05 to identify differentially expressed genes (DEGs) between the POI group and the control group. The results were presented through volcano plots and heatmaps generated using the "ggplot2" R package (version 3.3.2) and the "ComplexHeatmap" R package (version 2.10.0). Additionally, enrichment analysis of the selected DEGs was performed using the "clusterProfiler" R package (version 4.10.0), with the background selected from the KEGG. The results were visualized using the "ggplot2" R package.

Dual-luciferase reporter gene assay

Potential binding sites between AMPK and let-7a-5p were identified using TargetScan (http://www.targetscan.org). The let-7a-5p mimics/inhibitors and corresponding negative control (NC) were synthesized by Guangzhou RiboBio Co., Ltd. The amplified products were inserted into the pmirGLO vector (Promega, USA) between the SacI and XbaI restriction sites. Human embryonic kidney 293T cells (HEK293T) with low endogenous miRNA expression (Procell Life Science & Technology Co., Ltd., China) were selected. Using Lipofectamine 2000 (Invitrogen, USA), 800 ng of wild-type or mutant reporter gene was combined with 20 μM let-7a-5p mimic/inhibitor and co-transfected into HEK293T cells. After 24 h of transfection, Firefly & Renilla luciferase activities were measured in the lysed HEK293T cells using a dual-luciferase reporter detection system (Promega, USA).

Immunofluorescent staining

The expressions of Beclin, p62, Cyp17a1, and FSHR were detected using immunofluorescence staining. Ovarian tissue or TICs frozen sections from each group were fixed and then incubated overnight at 4 °C with primary antibodies: anti-Beclin (1:150), anti-p62 (1:150), anti-Cyp17a1 (1:100), and anti-FSHR (1:100). The next day, the tissue sections and TICs were allowed to warm to room temperature for 0.5 h, followed by a 1-hour incubation with secondary antibodies: goat anti-rabbit IgG, Alexa Fluor 594 (Abbkine, China) and goat anti-mouse IgG, Alexa Fluor 488 (Abbkine, China). Sections were incubated with DAPI in the dark for 10 min and then observed under an inverted fluorescence microscope (Leica, Germany) for staining results.

CCK-8 cell viability assay

The impact of various concentrations of CTX on TICs activity was assessed using the CCK-8 kit (Biosharp, China). TICs (5×10^3 cells/well) were seeded in a 96-well plate. When the cells reached 80% confluence, the medium was replaced with a culture medium containing CTX (0–80 μM). The cells without CTX (0 μM) was used as the negative control group. After 24 h, the CCK-8 working solution was added to the cell culture medium and incubated for 1 h. Absorbance was then measured at 450 nm to determine cell viability.

Western blot

Ovarian tissue and cultured TICs were lysed using radioimmunoprecipitation (RIPA) buffer, and protein concentration was determined by the BCA method (Solarbio, China). Cell and tissue samples were subjected to electrophoresis on polyacrylamide gels and then transferred to PVDF membranes. After blocking the membranes with 5% non-fat milk, they were incubated overnight at 4 °C with primary antibodies against AMPK (1:1500), p-AMPK (1:1000), mTOR (1:1000), p-mTOR (1:1000), Beclin (1:2000), LC3 (1:1500), p62 (1:2000), or GAPDH (1:20000). The next day, membranes were washed with TBS and Tween 20 (TBST) and then incubated with HRP-conjugated secondary antibody (1:20000) at room temperature for 1 h. The expression of each protein was detected using an ECL kit, and band density was measured using ImageJ software (NIH, Bethesda).

Data analysis

Data were expressed as means ± SD and were analyzed with the use of SPSS 23.0 software. Independent sample t-tests were used for comparison between two groups,

and one-way analysis of variance (ANOVA) and post hoc Bonferroni test were used for comparison between more than two groups to evaluate the differences between groups. The difference was considered statistically significant when $P < 0.05$ for the experimental data.

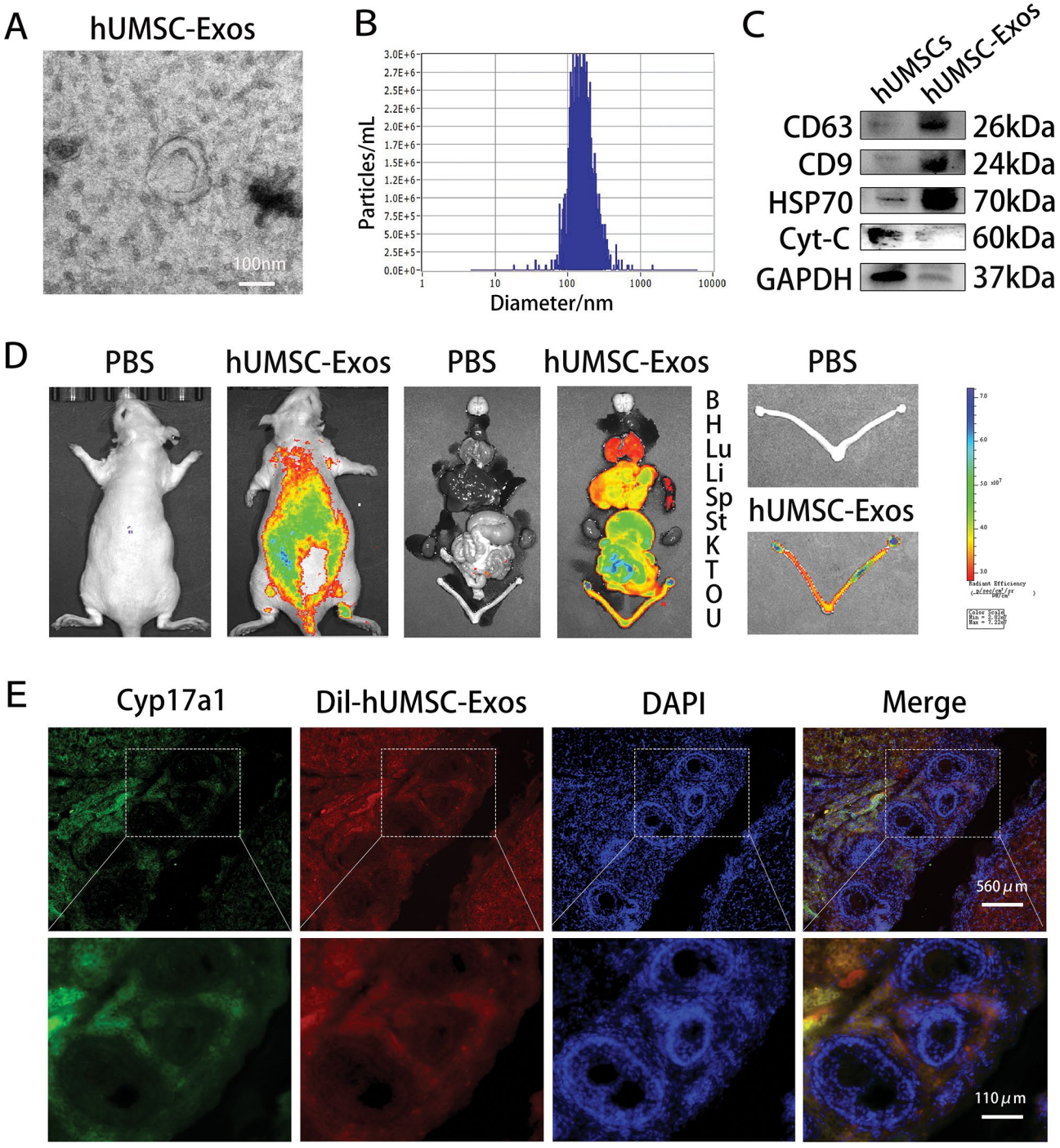

Fig. 1 Identification and tracking of hUMSC-Exos. (**A**) Morphological structure of hUMSC-Exos under electron microscope (scale bar = 100 nm). (**B**) The diameter of hUMSC-Exos was determined by NTA. (**C**) The expression of exosome-positive markers CD63, CD9, and HSP70 and negative exosome markers Cyt-C were detected by western blot. Full-length blots are presented in Additional file 2. (**D**) Fluorescence intensity expression of rats and anatomical organs in vivo imaging. (**E**) Immunofluorescence images showed the accumulation of Dil-labeled hUMSC-Exos in the ovarian tissue of rats (scale bar = 560 μm and 110 μm)

Results

Identification and tracking of hUMSC-Exos

Under electron microscopy, typical disk-shaped particles with diameters of 70–200 nm were observed, further confirmed by NTA results (Fig. 1A-B). As shown in Fig. 1C, western blot assays revealed that the surface-specific positive markers CD63, CD9, and HSP70 were highly expressed in the exosomes from hUMSCs. The expression levels of GAPDH and Cyt-C were found to be lower in hUMSC-Exos when compared to hUMSCs. Following the tail vein injection of Dil-labeled hUMSC-Exos, in vivo tracking revealed a high accumulation of hUMSC-Exos in the thoracic and abdominal regions as well as in both ovaries of the rats (Fig. 1D). Further immunofluorescence staining of the TICs marker Cyp17a1 indicated significant overlap between Dil-labeled exosomes and Cyp17a1 in rat ovarian tissue, particularly within the TICs (Fig. 1E). These findings suggested that hUMSC-Exos exhibit ovarian tropism in vivo and can be taken up by TICs.

hUMSC-Exos repairs ovarian dysfunction in POI rats

After a one-week acclimatization period, rats with normal estrous cycles were selected for subsequent experiments (Fig. 2A). The body weight and wet ovarian weight of each group were recorded and analyzed over 26 days post-transplantation. As shown in Fig. 2B-C, the POI group exhibited slow weight gain and a decreasing trend in wet ovarian weight compared to the control group. However, the body weight and wet ovarian weight were significantly improved after the transplantation of hUMSC-Exos in POI rats.

Morphological changes in the ovaries of each group were observed through H&E staining. As shown in Fig. 2D-E, the number of functional follicles decreased and the number of corpora lutea increased in the POI group. However, after hUMSC-Exos treatment, the number of functional follicles significantly increased, accompanied by the reappearance of mature follicles, while the numbers of corpora lutea and degenerated follicles significantly decreased. Then, the serum hormone levels were measured to evaluate the ovarian function status. Compared to the control group, the levels of AMH and E_2 in the POI group were significantly lower, while the levels of LH and FSH were significantly higher. Following hUMSC-Exos treatment, the abnormal hormone levels in POI rats were significantly restored (Fig. 2F-I).

Additionally, fertility experiments were conducted to observe the ovarian function of the rats. As shown in Fig. 2J-K, the number of implanted rats in the POI group was significantly lower than that in the control group. However, hUMSC-Exos transplantation reversed this situation. The above results suggested that in vivo intervention with hUMSC-Exos alleviates ovarian morphological and functional abnormalities and improves reproductive ability in POI rats.

hUMSC-Exos inhibits autophagy of ovarian tissue by regulating the AMPK/mTOR pathway in POI rats

The transcriptome data of ovarian tissues from the POI group and normal control group in the GSE 217,193 dataset were analyzed, and a total of 1056 DEGs were identified ($LogFC > 0.05$ and $p\text{-value} < 0.05$), including 764 up-regulated genes and 292 down-regulated genes (Fig. 3A-B). Notably, the autophagy signaling pathway was enriched in DEGs by KEGG analysis (Fig. 3C).

To uncover the potential mechanism by which hUMSC-Exos alleviates ovarian structural and functional abnormalities in POI rats, we examined the AMPK/mTOR pathway-mediated autophagy. Compared to the control group, the POI group showed a significant increase in AMPK level and the p-AMPK/AMPK ratio, and a significant decrease in the p-mTOR/mTOR ratio (Fig. 3E-H). Furthermore, the hUMSC-Exos intervention dramatically reversed the expression of AMPK/mTOR pathway-mediated autophagy-related molecules. As shown in Fig. 3E, I-K, compared to the control group, the level of Beclin and the ratio of LC3II / LC3I were significantly increased, and the level of p62 was significantly decreased in the POI group. The analysis results of autophagy-related molecules p62 and Beclin by immunofluorescence staining are consistent with the above results (Fig. 3L). These results indicated that in POI rats, hUMSC-Exos suppresses autophagy of ovarian tissue by modulating the AMPK/mTOR pathway.

hUMSC-Exos alleviates tics autophagy by targeting the AMPK/mTOR pathway

The TICs were isolated from rat ovarian tissue to explore the molecular mechanisms by which hUMSC-Exos regulates TICs autophagy. Identification of extracted cell types using immunofluorescence staining with TICs and GCs marker molecule (Cyp17a1 and FSHR). Cells that were Cyp17a1 positive and FSHR negative were identified as the TICs (Fig. 4A). Furthermore, the hormone secretion capacity of TICs was confirmed by measuring the levels of T and E_2 hormones (Fig. 4B). To analyze the cytotoxic effect of CTX, TICs were exposed to gradient concentrations of CTX (0–80 μM). The cells without CTX (0 μM) was used as the negative control group. The CCK-8 assay was utilized to establish the appropriate CTX concentration (40 μM) for constructing an in vitro damage model (Fig. 4C). Additionally, by culturing TICs and Dil-labeled hUMSC-Exos for 60 min, it was observed that TICs exhibited Dil labeling, indicating its internalization of hUMSC-Exos (Fig. 4D).

Using the extracted TICs, we further explored the mechanism by which hUMSC-Exos regulates TICs

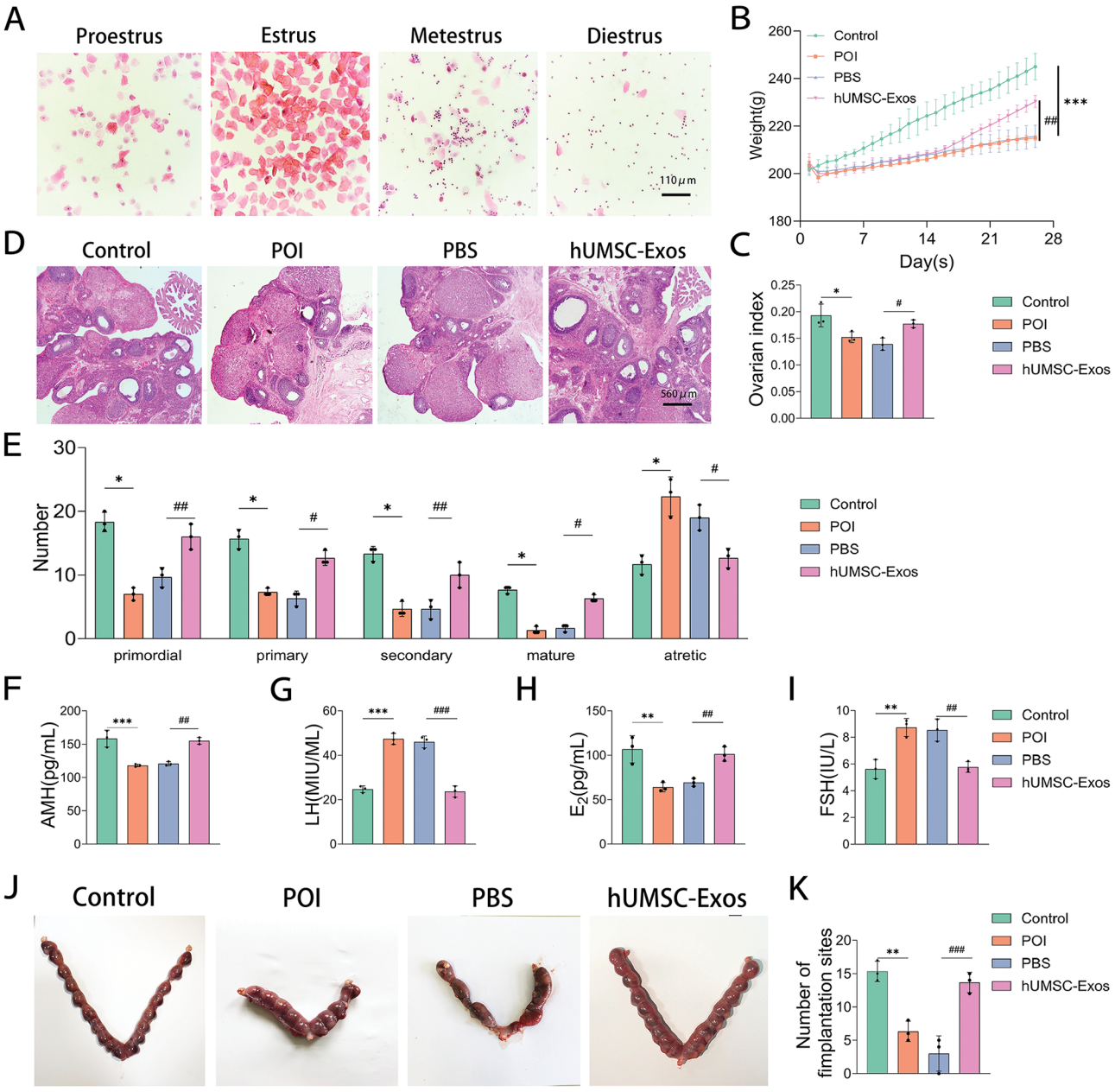

Fig. 2 hUMSC-Exos alleviate ovarian morphology and function in POI rats. (**A**) The estrous cycle of rats (scale bar = 110 μm). (**B**) Mean body weight. (**C**) Mean ovarian index. (**D**) Representative images of the ovaries (scale bar = 560 μm). (**E**) The number of follicles in different developmental stages of ovaries. (**F**-**I**) Levels of AMH, LH, E_2, and FSH hormones in serum. (**J**) Gross observation of uterine implantation. (**K**) The number of implantation sites in rats. The data are presented as the means ± SEMs of at least three independent experiments. *$p < 0.05$, **$p < 0.01$ and ***$p < 0.001$, Control group vs. POI group; #$p < 0.05$, ##$p < 0.01$ and ###$p < 0.001$, PBS group vs. hUMSC-Exos group

autophagy by targeting the AMPK/mTOR pathway. As shown in Fig. 5B-E, compared to the control group, the AMPK level and p-AMPK/AMPK ratio were significantly increased in the CTX group, while the p-mTOR/mTOR ratio was significantly decreased. Similarly, the Beclin level and LC3II / LC3I ratio were significantly elevated and the p62 level was markedly decreased in the CTX group compared to the control group (Fig. 5B, F-H). In contrast, the levels of these autophagy-related proteins showed opposite results in the hUMSC-Exos treatment group (Fig. 5B, F-H). The analysis results of autophagy-related molecules p62 and Beclin by immunofluorescence staining were consistent with the above results (Fig. 5K). Furthermore, the detection of let-7a-5p and AMPK miRNA/mRNA levels indicated that hUMSC-Exos intervention significantly upregulated the let-7a-5p level and significantly downregulated the AMPK mRNA levels in CTX-damaged TICs (Fig. 5I-J). These findings suggested

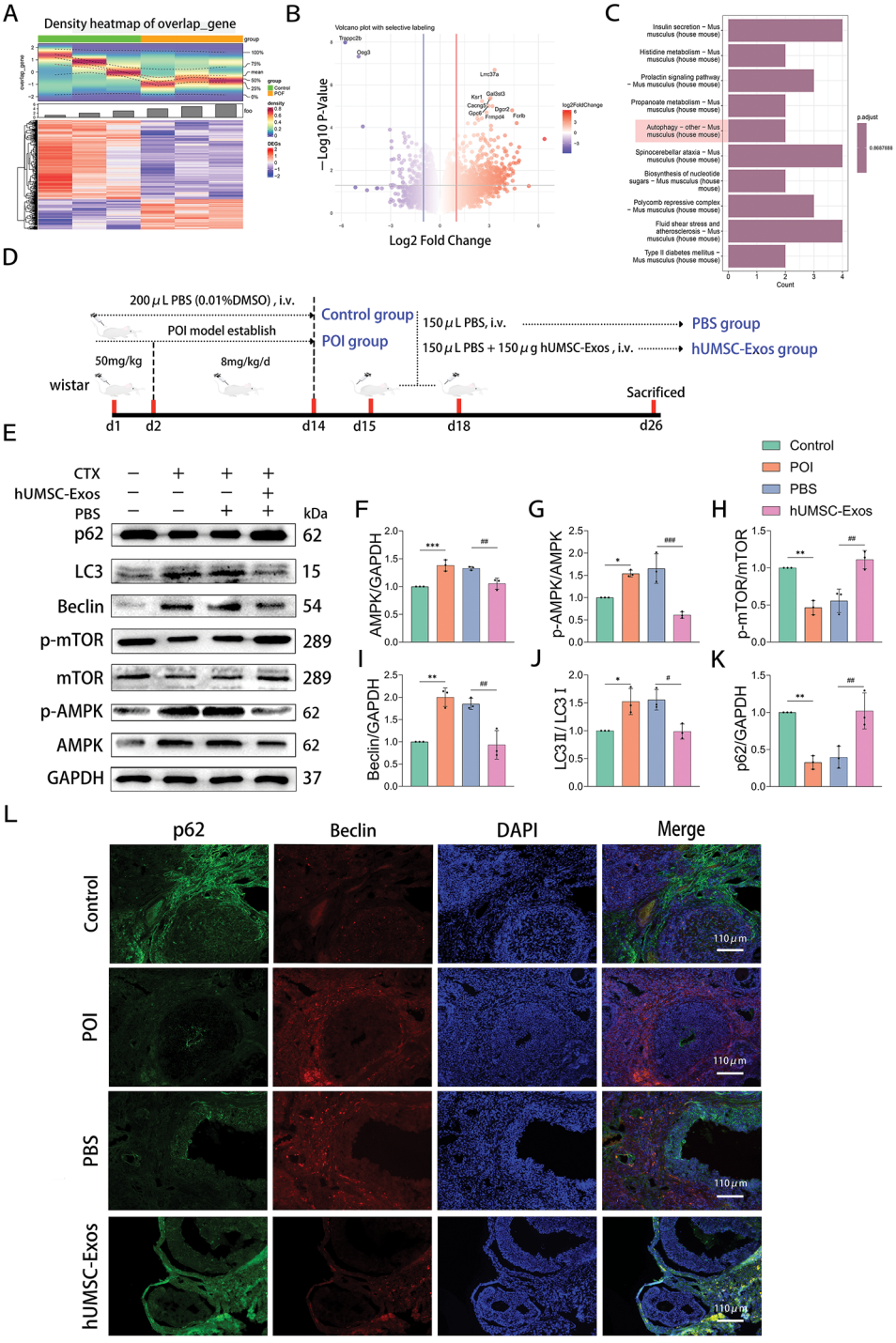

Fig. 3 hUMSC-Exos suppresses autophagy of ovarian tissue by modulating the AMPK/mTOR pathway. (**A**) Heatmap of differentially expressed genes (DEGs) in the ovarian insufficiency group and the normal ovarian group. (**B**) Volcano plot of all DEGs in the ovarian insufficiency group and the normal ovarian group. (**C**) KEGG pathway enrichment analysis for the selected DEGs. (**D**) The scheme shows the experimental design. (**E**) The expression of the AMPK/mTOR pathway and autophagy-related proteins were detected by western blot. Full-length blots are presented in Additional file 2. (**F**) AMPK protein level. (**G**) p-AMPK/ AMPK ratio. (**H**) p-mTOR/mTOR ratio. (**I**) Beclin protein level. (**J**) LC3II / LC3I ratio. (**K**) p62 protein level. (**L**) The expression of p62 and Beclin were tested by immunofluorescence staining (scale bar = 110 μm). The data are presented as the means ± SEMs of at least three independent experiments. *$p < 0.05$, **$p < 0.01$ and ***$p < 0.001$, Control group vs. POI group; #$p < 0.05$, ##$p < 0.01$ and ###$p < 0.001$, PBS group vs. hUMSC-Exos group

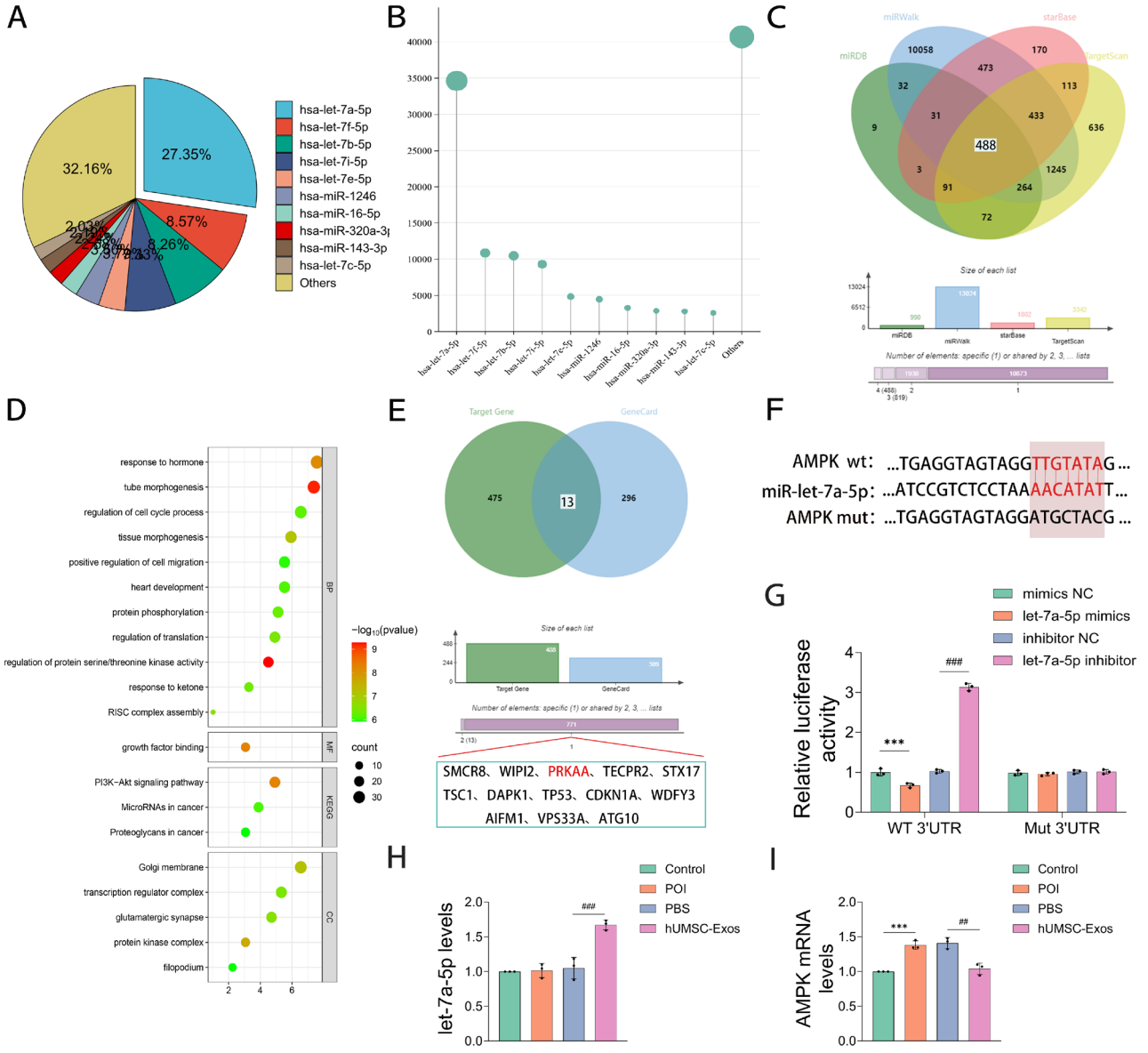

Fig. 4 Separation and identification of TICs. (**A**) The expression levels of Cyp17a1 and FSHR were detected by immunofluorescence (scale bar = 220 μm). (**B**) The levels of T and E_2 in the supernatant were detected by ELISA. (**C**) The effect of different concentrations of CTX on TICs viability were determined. (**D**) Dil-labeled hUCMSC-Exo were internalized by TICs (scale bar = 220 μm). Data are presented as means ± SEMs of at least three independent experiments

that hUMSC-Exos intervention alleviates CTX-induced TICs autophagy associated with the AMPK/mTOR pathway, potentially involving the transfer of let-7a-5p.

let-7a-5p is enriched in hUMSC-Exos and targets AMPK

To assess the miRNA expression profile of hUMSC-Exos and the therapeutic mechanism, miRNAs were screened using miRNA-seq. Notably, the top ten most abundant miRNAs were let-7a-5p, let-7f-5p, let-7b-5p, let-7i-5p, let-7e-5p, miR-1246, miR-16-5p, miR-320a-3p, miR-143-3p, and let-7c-5p, which together accounted for 67.84% of the total (Fig. 6A-B). As shown in Fig. 6C, we predicted and intersected the target genes of let-7a-5p using the miRDB, miRWalk, starBase, and TargetScan databases, identifying a total of 488 genes. In addition, the enrichment analysis of the identified target genes for BP, MF, KEGG, and CC showed that the pathways associated with autophagy include the regulation of protein phosphorylation, regulation of protein kinase complexes, and the PI3K/Akt signaling pathway (Fig. 6D). When the 488 predicted target genes of let-7a-5p were intersected with 310 autophagy-related genes, 13 genes were identified, including the key autophagy molecule AMPK (Fig. 6E). These results indicated that the mechanism of POI occurrence is related to autophagy regulation, with AMPK playing a crucial role.

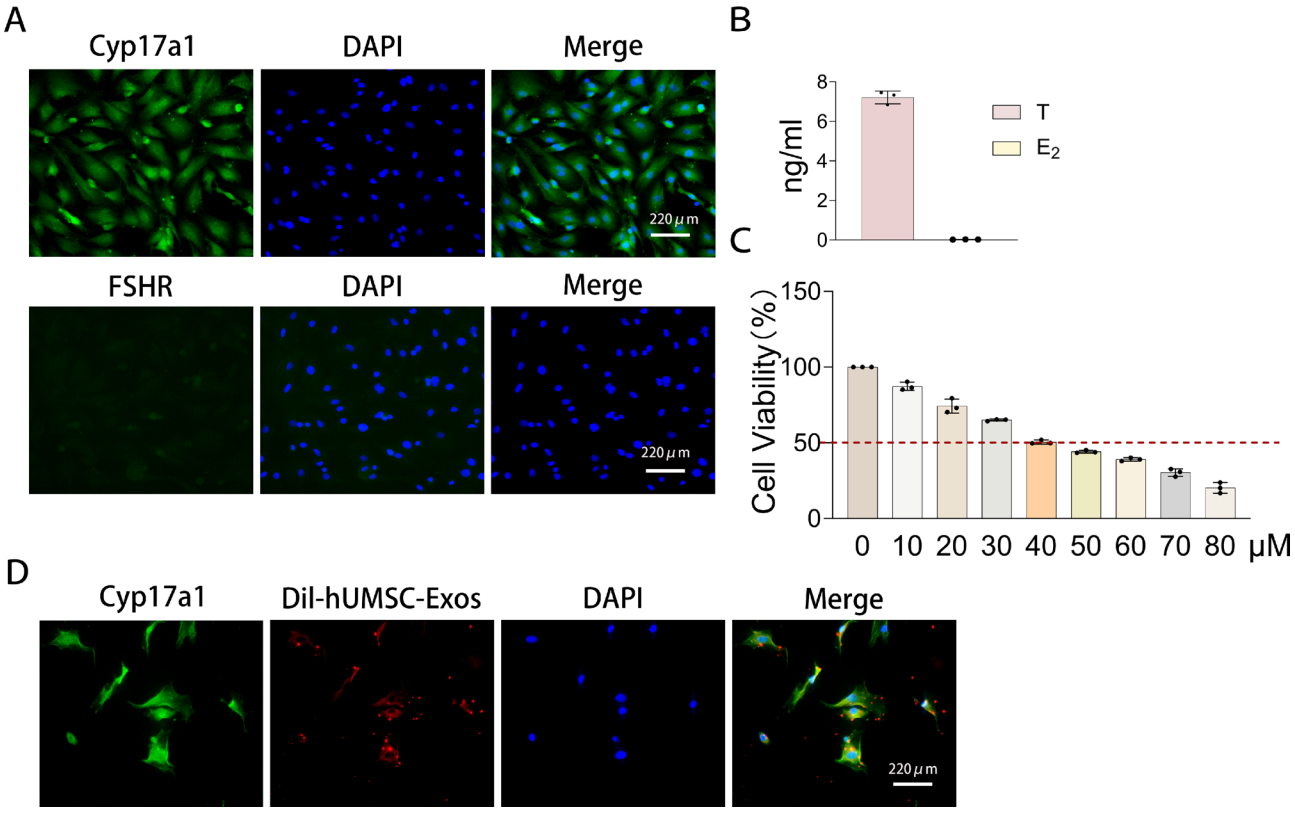

Fig. 5 hUMSC-Exos alleviates TICs autophagy by targeting the AMPK/mTOR pathway. (**A**) The scheme shows the experimental design. (**B**) The expression of the AMPK/mTOR pathway and autophagy-related proteins were detected by western blot. Full-length blots are presented in Additional file 2. (**C**) AMPK protein level. (**D**) p-AMPK/AMPK ratio. (**E**) p-mTOR/mTOR ratio. (**F**) Beclin protein level. (**G**) LC3II / LC3I ratio. (**H**) p62 protein level. (**I**) The level of let-7a-5p was detected by qRT-PCR. (**J**) The level of AMPK mRNA was detected by qRT-PCR. (**K**) The expression levels of p62 and Beclin were detected by immunofluorescence (scale bar = 560 μm). Data are presented as means ± SEMs of at least three independent experiments. *$p < 0.05$, ***$p < 0.001$, Control group vs. CTX group; #$p < 0.05$, ##$p < 0.01$ and ###$p < 0.001$, CTX group vs. hUMSC-Exos group

Subsequently, to verify if AMPK is a target gene of let-7a-5p, we employed a dual-luciferase reporter experiment to locate the let-7a-5p binding site in AMPK (Fig. 6F). Compared to the control group, the luciferase activity in the let-7a-5p mimic group was reduced, while it significantly increased after treatment with the let-7a-5p inhibitor (Fig. 6G). Additionally, qRT-PCR further confirmed that let-7a-5p expression significantly increased in the ovaries of POI rats after hUMSC-Exos transplantation (Fig. 6H). As shown in Fig. 6I, the AMPK mRNA expression was significantly increased in the POI group compared to the control but decreased after hUMSC-Exos intervention. These results indicated that let-7a-5p-mediated suppression of AMPK could be a viable way for hUMSC-Exos to ameliorate POI-induced autophagy.

The delivery of let-7a-5p is key for hUMSC-Exos to regulate autophagy of tics by targeting the AMPK/mTOR pathway

To confirm the role of let-7a-5p in TICs in regulating AMPK/mTOR pathway and autophagy, TICs were treated with different plasmids (inhibitor NC, let-7a-5p inhibitor, mimic NC and let-7a-5p mimic). As shown in Fig. 7B-H, compared with inh-NC group, AMPK level, p-AMPK/AMPK ratio, Beclin level and LC3II/ LC3I ratio were markedly increased in inh-let-7a-5p group, while p-mTOR/mTOR ratio and p62 level were markedly decreased in inh-let-7a-5p group. In addition, compared with mimic-NC group, AMPK level, p-AMPK/AMPK ratio, Beclin level and LC3II/ LC3I ratio were significantly decreased in mimic-let-7a-5p group, while p-mTOR/mTOR ratio and p62 level were significantly increased in mimic-let-7a-5p group (Fig. 7B-H). In addition, let-7a-5p levels were markedly lower and AMPK mRNA levels were significantly higher in the inh-let-7a-5p group than in the ihn-NC group (Fig. 7I-J). In contrast, let-7a-5p levels were significantly higher and AMPK mRNA levels were greatly lower in the mimic-let-7a-5p group than in the mimic-NC group (Fig. 7I-J).

Finally, to further validate the above hypothesis, hUMSCs were treated with different plasmids (inhibitor NC, let-7a-5p inhibitor, mimic NC and let-7a-5p mimic). The supernatants were collected, and hUMSC-Exos were extracted. Then, hUMSC-Exos from the inhibitor NC

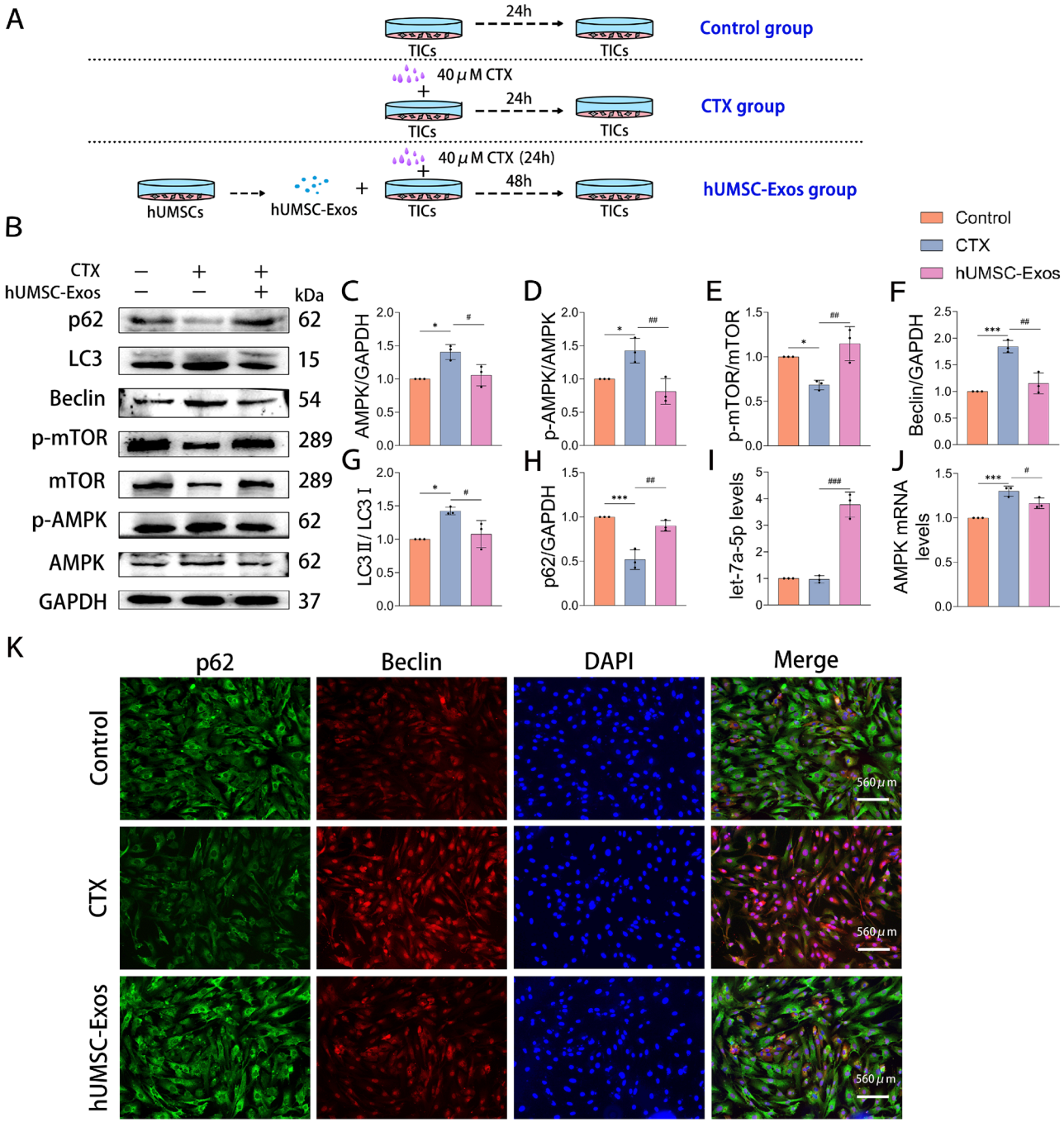

Fig. 6 let-7a-5p can target and negatively regulate AMPK. (**A**-**B**) Pie and lollipop charts show the top 10 most abundant miRNAs in hUMSC-Exos according to miRNA-seq results. (**C**) Venn diagram of the intersection of the predicted target genes of let-7a-5p. (**D**) BP, MF, KEGG, and CC enrichment analysis for the predicted intersection. (**E**) Venn diagram showing the intersection of let-7a-5p target genes and autophagy pathway-related genes. (**F**) TargetScan was used to predict the binding site of let-7a-5p in the AMPK 3′-UTR. (**G**) Luciferase activity was measured using a dual-luciferase reporter gene assay. (**H**) The mRNA expression of let-7a-5p was detected by qRT-PCR. (**I**) The mRNA expression of AMPK was detected by qRT-PCR. Data are presented as means ± SEMs of at least three independent experiments. *$p < 0.05$, **$p < 0.01$ and ***$p < 0.001$, #$p < 0.05$, ##$p < 0.01$ and ###$p < 0.001$

group, let-7a-5p inhibitor group, mimic NC group and let-7a-5p mimic group were co-cultured with TICs under a CTX (40 μM) intervention environment. As shown in Fig. 8B-E, compared to the inh-NC group, the AMPK level and p-AMPK/AMPK ratio in the inh-let-7a-5p group were significantly higher, while the p-mTOR/mTOR ratio was significantly lower in the inh-let-7a-5p group. In addition, the Beclin level and LC3II / LC3I ratio were significantly elevated and the p62 level was markedly decreased in the inh-let-7a-5p group compared

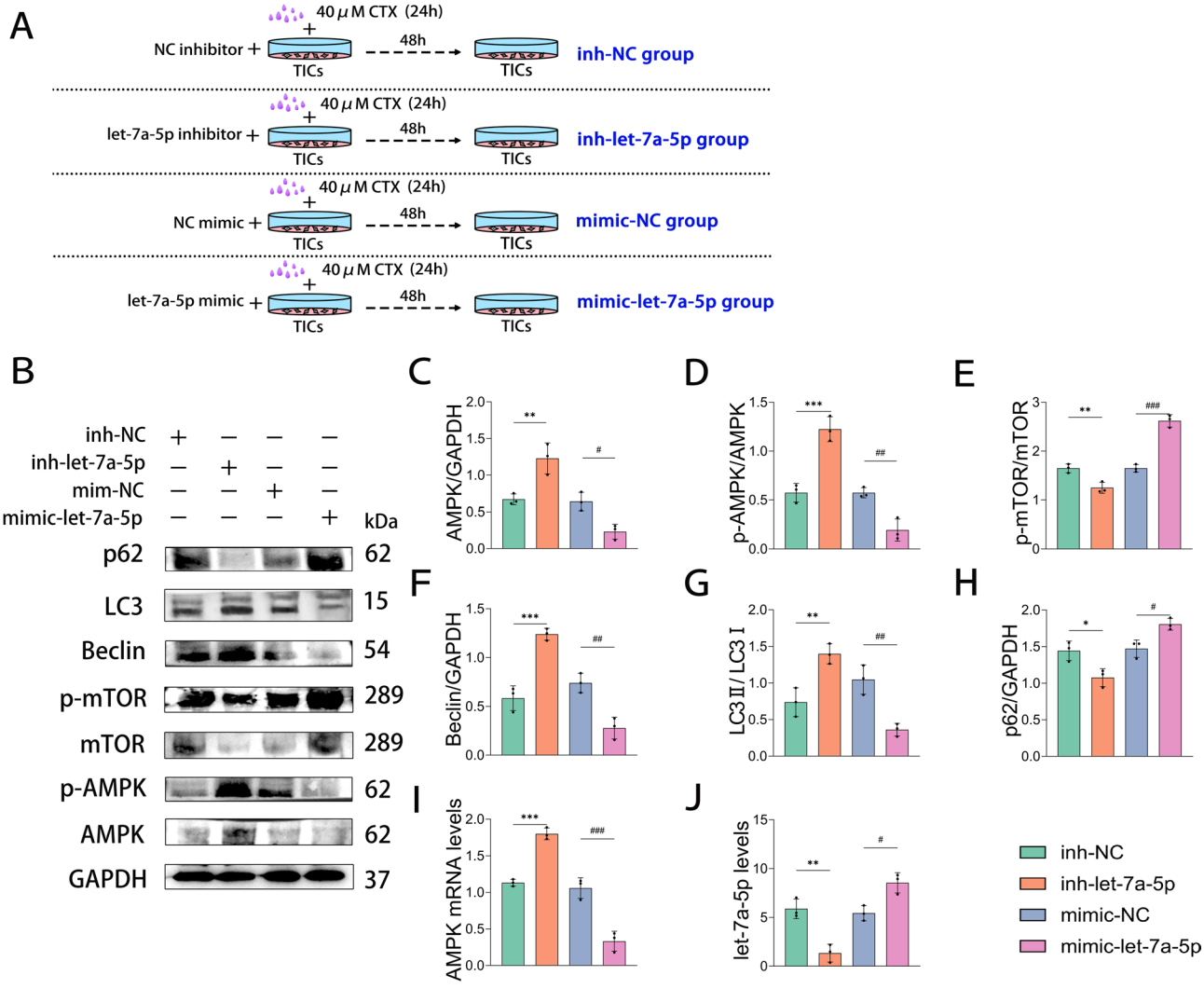

Fig. 7 let-7a-5p in TICs can regulate AMPK/mTOR pathway and TICs autophagy. (**A**) The scheme shows the experimental design. (**B**) The expression of the AMPK/mTOR pathway and autophagy-related proteins were detected by western blot. Full-length blots are presented in Additional file 2. (**C**) AMPK protein level. (**D**) p-AMPK/AMPK ratio. (**E**) p-mTOR/mTOR ratio. (**F**) Beclin protein level. (**G**) LC3II / LC3I ratio. (**H**) p62 protein level. (**I**) The mRNA expression of AMPK was measured by qRT-PCR. (**J**) The level of let-7a-5p was measured by qRT-PCR. Data are presented as the means ± SEMs of at least three independent experiments. $^{*}p<0.05$, $^{**}p<0.01$ and $^{***}p<0.001$, inh-let-7a-5p group vs. inh-NC group. $^{\#}p<0.05$, $^{\#\#}p<0.01$ and $^{\#\#\#}p<0.001$, mimic-let-7a-5p group vs. mimic-NC group

to the NC group (Fig. 8B, F-H). Meanwhile, as shown in Fig. 8B-E, compared with the mimic-NC group, the AMPK level and p-AMPK/AMPK ratio in the mimic-let-7a-5p group were greatly lower, while the p-mTOR/mTOR ratio in the mimic-let-7a-5p group was significantly higher. Furthermore, Beclin level and LC3II/ LC3I ratio were significantly decreased and p62 level was greatly increased in mimic-let-7a-5p group compared with mimic-NC group (Fig. 8B, F-H). And the analysis results of autophagy-related molecules p62 and Beclin by immunofluorescence staining are consistent with the above results (Fig. 8K). Furthermore, compared to the ihn-NC group, the level of let-7a-5p was significantly lower and the AMPK mRNA level was significantly higher in the inh-let-7a-5p group (Fig. 8I-J). Conversely, let-7a-5p levels were markedly higher and AMPK mRNA levels were significantly lower in the mimic-let-7a-5p group than in the mimic-NC group (Fig. 8I-J). These findings indicated that the transport of let-7a-5p is critical for hUMSC-Exos to regulate TICs autophagy by targeting the AMPK/mTOR pathway.

Discussion

Due to the benefits of encouraging tissue repair, angiogenesis, and anti-aging, MSC-Exos received a lot of consideration in POI treatment [21]. Recently, an enormous quantity of literature and our investigations have revealed that hUMSCs and their derived exosomes regulate the

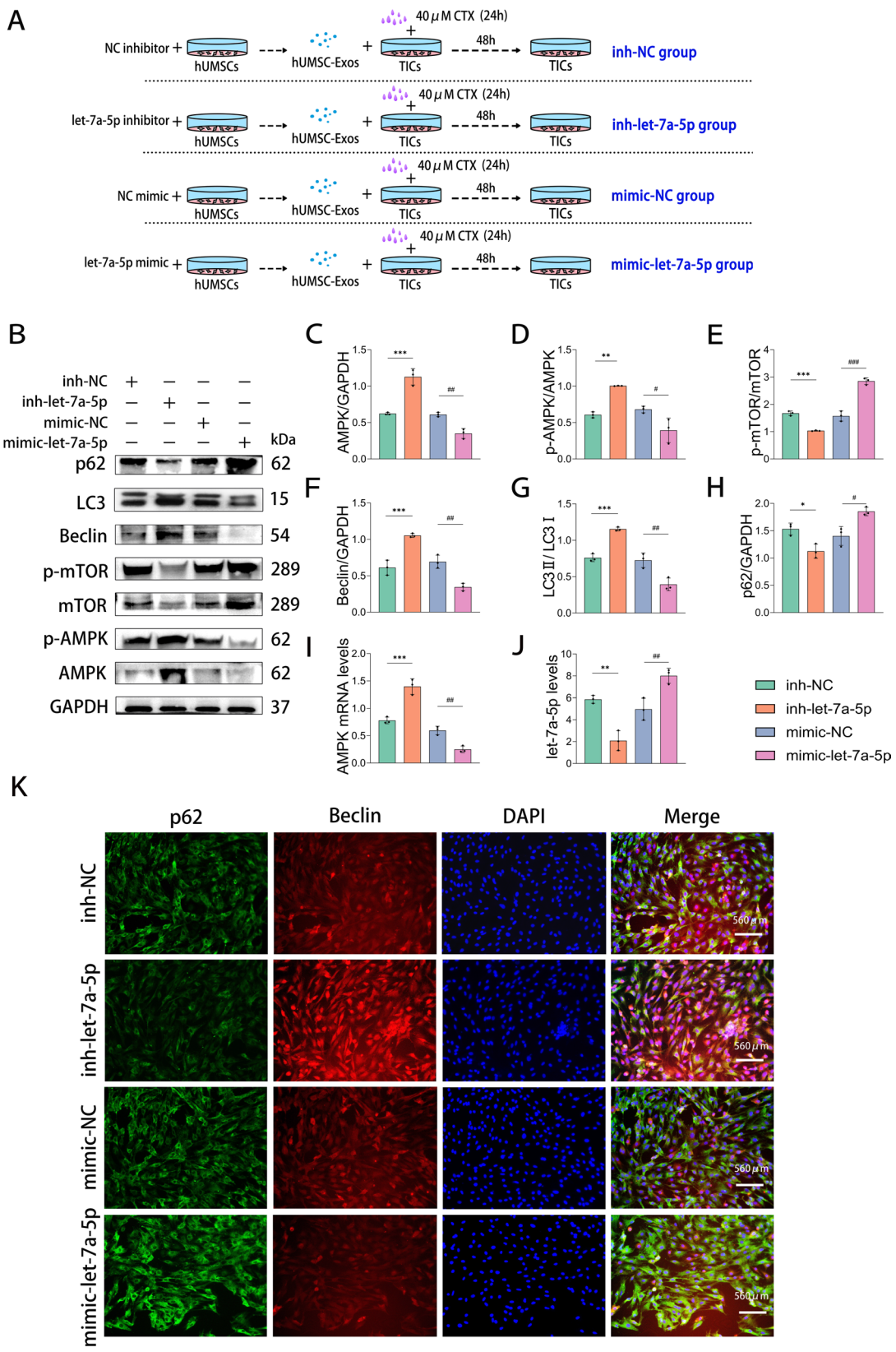

Fig. 8 (See legend on next page.)

(See figure on previous page.)

Fig. 8 hUMSC-Exos regulates autophagy of TICs via let-7a-5p transmission. (**A**) The scheme shows the experimental design. (**B**) The expression of the AMPK/mTOR pathway and autophagy-related proteins were detected by western blot. Full-length blots are presented in Additional file 2. (**C**) AMPK protein level. (**D**) p-AMPK/AMPK ratio. (**E**) p-mTOR/mTOR ratio. (**F**) Beclin protein level. (**G**) LC3II / LC3I ratio. (**H**) p62 protein level. (**I**) The mRNA expression of AMPK was measured by qRT-PCR. (**J**) The level of let-7a-5p was measured by qRT-PCR (**K**) The expressions of p62 and Beclin were detected by immunofluorescence (scale bar = 560 μm). Data are presented as the means ± SEMs of at least three independent experiments. $^{*}p < 0.05$, $^{**}p < 0.01$ and $^{***}p < 0.001$, inh-let-7a-5p group vs. inh-NC group. $^{\#}p < 0.05$, $^{\#\#}p < 0.01$ and $^{\#\#\#}p < 0.001$, mimic-let-7a-5p group vs. mimic-NC group

metabolism of ovarian tissue cells and play a vital role in the therapy of POI [22, 23]. Our current study has shown that hUMSC-Exos reduced ovarian damage in POI rats by suppressing TICs autophagy. In addition, the therapeutic effect of hUMSC-Exos on POI was primarily achieved by delivering let-7a-5p, which targets the AMPK/mTOR autophagy pathway. Our findings are expected to yield new therapeutic targets and strategies for the clinical treatment of POI.

The significant aging and death of ovarian cells caused by chemotherapy drugs, immune factor abnormalities, chromosomal abnormalities, and other factors are the main causes of clinical POI. Chen et al. demonstrated that CTX disrupts GCs mitochondrial function, which leads to ovarian dysfunction and the emergence of POI [24]. Hu et al. discovered that CTX causes POI by activating the IL-17 A/IL-6 signaling axis and inducing downstream MEK/ERK activity of ovarian tissue [25]. In this research, we noticed that as compared to the control group, the POI group rats had a lower body weight, lower ovarian wet weight, and a significantly reduced amount of functional follicles. AMH and E_2 levels in the serum of POI group rats were substantially decreased, but LH and FSH levels were significantly increased. In addition, the quantity of embryos in POI rats' uteruses reduced considerably. In vitro investigations revealed that CTX treatment activated an increase in autophagy-related molecules in TICs compared with the control group. In this investigation, we revealed that autophagy in TICs may also serve as a trigger for POI. Mature TICs can increase follicle sensitivity to gonadotropins and boost the stimulating influence of growth factors in the blood on follicle development [26, 27]. When TICs are destroyed, androgen and growth factor release is severely reduced, and GCs are unable to synthesize estrogen, resulting in follicle developmental problems and POI owing to atresia [28]. As a consequence, aberrant TICs metabolism could be a significant trigger for CTX-induced structural and functional abnormalities in POI ovaries.

Autophagy is a regulated autocrine activity in cells that is crucial for cell growth, metabolism, and other functions that maintain balance and homeostasis [29]. The AMPK signaling pathway, as one of the primary autophagy signaling pathways, has been extensively investigated in a variety of female reproductive diseases [20, 30]. Yang et al. found that metformin protects GCs from chemotherapy-induced damage, reduces oxidative damage, and inflammation via activating the AMPK/PPAR-γ/SIRT1 pathway [31]. We also discovered that in vivo investigations, autophagy-associated molecules such as Beclin and LC3B-II protein levels increased while p62 levels dropped in POI rats. Furthermore, AMPK was activated whereas mTOR expression was suppressed. Similarly, in vitro tests showed that CTX-treated TICs increased autophagy-associated molecules and activated AMPK signaling pathway. This suggested that CTX-induced autophagy in TICs may be mediated through the AMPK/mTOR pathway during POI.

The unique functionality, targeting, and stability of MSC-Exos are critical for managing intercellular communication [32]. Recent investigations have demonstrated that MSC-Exos possesses anti-aging, anti-apoptosis, and anti-oxidation properties [33]. Ebrahim et al. found that bone mesenchymal stem cell-derived exosomes (BMSC-Exos) regulated autophagy via the PI3K/AKT/mTOR pathway, enhanced Aβ breakdown, regulated immunity, and improved memory and neuroaging [34]. In addition, Cao and colleagues discovered that ADSC-Exos targets Btg2 by transporting miRNA-21-5p, boosting the activation of the IRS1 and AKT pathways, which enhanced glucose metabolism in the liver, eventually rectifying the aberrant metabolism seen in polycystic ovary syndrome (PCOS) [35]. In this investigation, we revealed that hUMSC-Exos restored ovarian anatomy and promoted the formation of functional follicles in vivo. Compared to the PBS group, the hUMSC-Exos group rats had higher serum levels of E_2 and AMH, but lower levels of FSH and LH. Furthermore, after hUMSC-Exos treatment, the quantity of embryos in POI rats' uteruses rose, showing that ovarian function was restored. These findings demonstrated that hUMSC-Exos intervention in vivo can correct aberrant ovarian shape, function, and serum hormone levels, as well as restore ovarian function and reproductive potential in POI rats.

Numerous studies have shown that miRNA transmission is a critical channel for MSC-Exos to regulate intercellular signal transduction. Xiong et al. discovered that miRNA-21 supplied by human placental MSC-derived exosomes (hPMSC-Exo) regulated the PTEN/PI3K-Nrf2 axis and treated aging-related oxidative damage of $CD4^+$ T cells [36]. Sun et al. showed that BMSC-Exos delivered miR-644-5p targeting to control p53, suppress GCs apoptosis, and treated POI [37]. Through hUMSC-Exos transcriptome sequencing and double luciferase reporter

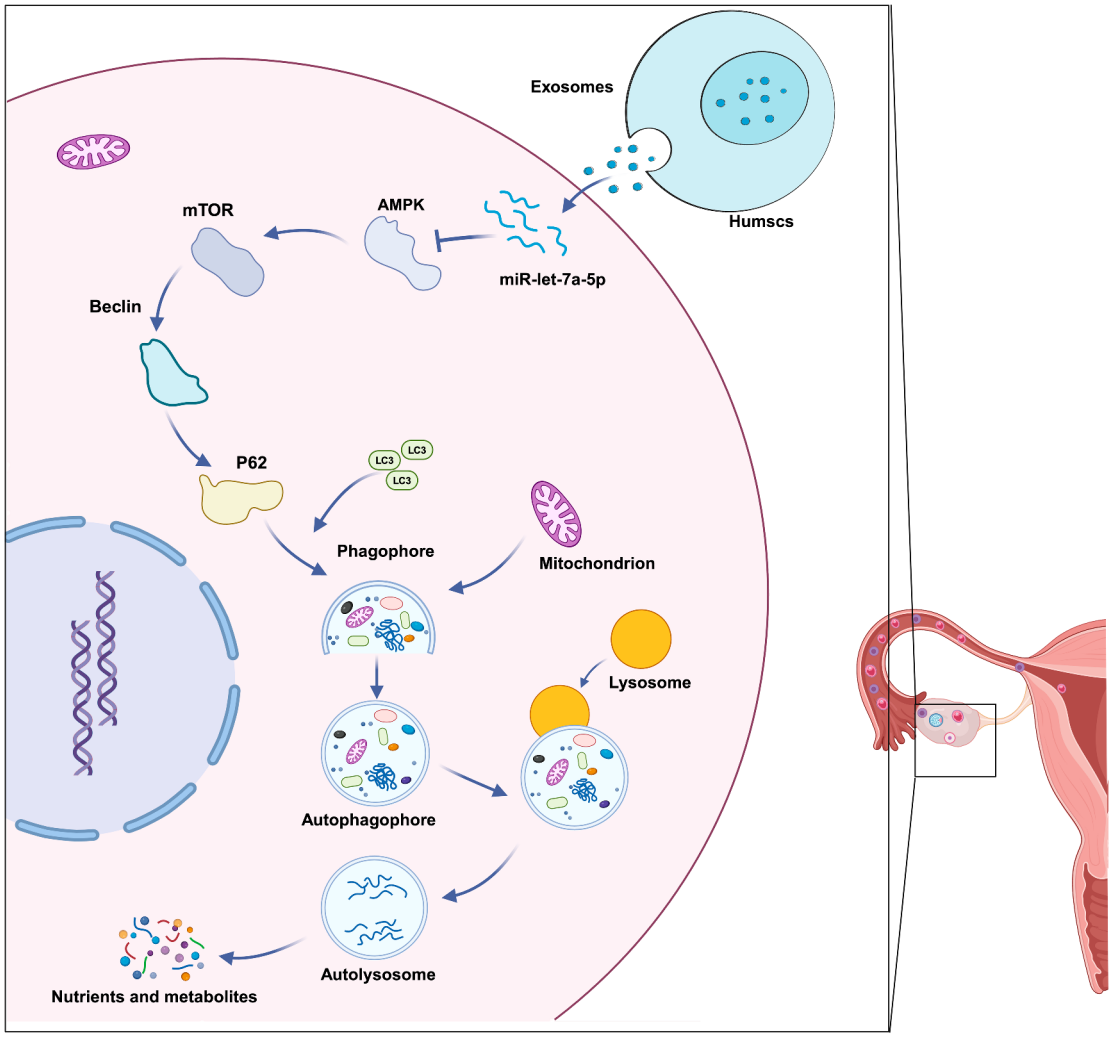

Fig. 9 Schematic diagram of protective effect of hUMSC-Exos on TICs in POI rats. hUMSC-Exos restored ovarian function in POI rats by delivering let-7a-5p and targeting AMPK/mTOR signaling pathway, blocking AMPK/mTOR axis-mediated autophagy in TICs

gene assays, we discovered that let-7a-5p, which was highly expressed in hUMSC-Exo, targets AMPK, a critical molecule controlling the autophagy pathway. In vivo tests revealed that hUMSC-Exos therapy dramatically increased the level of let-7a-5p in ovarian tissue while inhibiting the expression of autophagy-related markers. In addition, after knocking out or overexpressing let-7a-5p in exosomes in in vitro experiments, its regulatory effect on the autophagy pathway of TICs changed significantly. It is worth noting that after directly knocking out or overexpressing let-7a-5p in TICs, the molecules related to the autophagy pathway of TICs also showed corresponding significant changes. These results indicated that the translocation of let-7a-5p is essential for hUMSC-Exos to control TICs autophagy via the AMPK/mTOR pathway.

Although a large number of previous literatures have reported that the application of stem cell exosomes can alleviate the abnormalities in the structure and function of the ovary caused by factors such as oxidative stress, ferroptosis, and immune imbalance during the process of POI [6, 7, 38–40]. However, the regulatory effect of stem cell exosomes on the damage of TICs mediated by autophagy during the POI process remains unclear. Given the crucial role of TICs in the supply of follicular nutrients and the regulation of hormone secretion, the restoration of their metabolic function will be a key link in the treatment of POI [3]. Therefore, the innovative point of this study lies in the discovery of the molecular mechanism by which hUMSC-Exos alleviate ovarian damage in POI. Specifically, hUMSC-Exos target the autophagy pathway of TICs mediated by the AMPK/mTOR axis through the delivery of let-7a-5p.

Conclusion

In conclusion, our research indicates that, as shown in Fig. 9, hUMSC-Exos eliminates the dysfunction of ovarian structure and function during POI. The mechanism could be linked to suppressing AMPK/mTOR signaling-mediated autophagy of TICs and repairing aberrant hormone secretion and reproductive ability through the transfer of let-7a-5p. Our research opens up new avenues for studying the effects of hUMSCs on ovarian metabolism and could help identify new therapeutic targets and treatments for POI.

Abbreviations

POI	Premature ovarian insufficiency
hUMSCs	Human umbilical cord mesenchymal stem cells
EVs	Extracellular vesicles
hUMSC	Exos-Human umbilical cord mesenchymal stem cell derived exosomes
CTX	Cyclophosphamide
TICs	Theca interstitial cells
GCs	Granular cell
E_2	Estradiol
FSH	Follicle-stimulating hormone
LH	Luteinizing hormone
AMH	Anti-Mullerian hormone
T	Testosterone
GAPDH	Glyceraldehyde-3-phosphate dehydrogenase
AMPK	Amp-activated protein kinase
mTOR	Mammalian target of rapamycin

Supplementary Information

The online version contains supplementary material available at https://doi.org/10.1186/s13287-025-04396-1.

Supplementary Material 1

Supplementary Material 2

Acknowledgements

The authors declare that they have not use AI-generated work in this manuscript.

Author contributions

Yu Tang, Yu He, Xingyu Huo, Juntong Chen, Maojiao Qian, Haoyu Huang, Yixuan Meng, Lianshuang Zhang, Feibo Xu, Yukun Zhang, Hongchu Bao, Yanlian Xiong were all involved in the study design, data acquisition, and analysis. The authors read and approved the final manuscript.

Funding

This investigation was supported by the National Natural Science Foundation of China (No. 32200731); Natural Science Foundation of Shandong Province (No. ZR2021MC064 and ZR2021QH149); Shandong Province Higher Education Institutions "Youth Creative Team Program" Project (No. 2022KJ092); Xu Rongxiang Regenerative Medicine Development Plan Project (NO. BY2023XRX03).

Availability of data and materials

RNA-seq datasets have been uploaded to the NCBI Gene Expression Omnibus at accession no. GSE280447. Other data generated or analyzed in this study are included in this published article and its supplementary information files.

Declarations

Ethics approval and consent to participate

This study was approved by the Ethics Committee of Binzhou Medical University: Project title: Study on the mechanism of stem cell exosomes in treating premature ovarian failure (Approval number: No. 2023-24. Date of approval: June 23, 2023). We obtained the human umbilical cord from Affiliated Yantai Hospital of Binzhou Medical University. The participants provided written informed consent for the use of the samples (hUMSCs). The isolation and using of hUMSCs have been approved by the Ethics Committee of Affiliated Yantai Hospital of Binzhou Medical University (Approval number: 2022 – 121, Date of approval: October 15, 2022).

Consent for publication

Not applicable.

Competing interests

The authors declare that they have no conflict of interests.

Received: 1 November 2024 / Accepted: 14 May 2025
Published online: 07 June 2025

References

1. LING L, FENG X, WEI T, et al. Human amnion-derived mesenchymal stem cell (hAD-MSC) transplantation improves ovarian function in rats with premature ovarian insufficiency (POI) at least partly through a paracrine mechanism [J]. Stem Cell Res Ther. 2019;10(1):46.
2. SUN P, WANG H. Aberrant activation of KRAS in mouse theca-interstitial cells results in female infertility [J]. Front Physiol. 2022;13:991719.
3. LUO Q, TANG Y, JIANG Z, et al. hUCMSCs reduce theca interstitial cells apoptosis and restore ovarian function in premature ovarian insufficiency rats through regulating NR4A1-mediated mitochondrial mechanisms [J]. Reprod Biol Endocrinol. 2022;20(1):125.
4. LU X, BAO H, CUI L, et al. hUMSC transplantation restores ovarian function in POI rats by inhibiting autophagy of theca-interstitial cells via the AMPK/mTOR signaling pathway [J]. Stem Cell Res Ther. 2020;11(1):268.
5. DE VOS M, DEVROEY P. FAUSER B C. Primary ovarian insufficiency [J]. Lancet. 2010;376(9744):911–21.
6. ZHOU Y, HUANG J. Human mesenchymal stem cells derived exosomes improve ovarian function in chemotherapy-induced premature ovarian insufficiency mice by inhibiting ferroptosis through Nrf2/GPX4 pathway [J]. J Ovarian Res. 2024;17(1):80.
7. PU X, ZHANG L, ZHANG P, et al. Human UC-MSC-derived exosomes facilitate ovarian renovation in rats with chemotherapy-induced premature ovarian insufficiency [J]. Front Endocrinol (Lausanne). 2023;14:1205901.
8. GUO X, ZHU Y, GUO L, et al. BCAA insufficiency leads to premature ovarian insufficiency via ceramide-induced elevation of ROS [J]. EMBO Mol Med. 2023;15(4):e17450.
9. TAKAHASHI A, YOUSIF A. Premature ovarian insufficiency: pathogenesis and therapeutic potential of mesenchymal stem cell [J]. J Mol Med (Berl). 2021;99(5):637–50.
10. DOU X, YAN D, LIU S et al. Thymol alleviates LPS-Induced liver inflammation and apoptosis by inhibiting NLRP3 inflammasome activation and the AMPK-mTOR-Autophagy pathway [J]. Nutrients, 2022, 14(14).
11. KIM K H, LEE MS. Autophagy–a key player in cellular and body metabolism [J]. Nat Rev Endocrinol. 2014;10(6):322–37.
12. MIZUSHIMA N. Autophagy: renovation of cells and tissues [J]. Cell. 2011;147(4):728–41.
13. KUMAR M A, BABA S K, SADIDA H Q, et al. Extracellular vesicles as tools and targets in therapy for diseases [J]. Signal Transduct Target Ther. 2024;9(1):27.
14. YANG G, ZHANG B, XU M, et al. Improving granulosa cell function in premature ovarian failure with umbilical cord mesenchymal stromal cell Exosome-Derived Hsa_circ_0002021 [J]. Tissue Eng Regen Med. 2024;21(6):897–914.
15. QU Q, LIU L, CUI Y, et al. miR-126-3p containing exosomes derived from human umbilical cord mesenchymal stem cells promote angiogenesis and attenuate ovarian granulosa cell apoptosis in a preclinical rat model of premature ovarian failure [J]. Stem Cell Res Ther. 2022;13(1):352.
16. GU X, LI Y, CHEN K, et al. Exosomes derived from umbilical cord mesenchymal stem cells alleviate viral myocarditis through activating AMPK/mTOR-mediated autophagy flux pathway [J]. J Cell Mol Med. 2020;24(13):7515–30.

17. REN Y, HE J, WANG X, et al. Exosomes from adipose-derived stem cells alleviate premature ovarian failure via blockage of autophagy and AMPK/mTOR pathway [J]. PeerJ. 2023;11:e16517.
18. XIONG Y, SI Y, QUAN R, et al. hUMSCs restore ovarian function in POI mice by regulating GSK3beta-mediated mitochondrial dynamic imbalances in theca cells [J]. Sci Rep. 2024;14(1):19008.
19. LI W, SI Y, WANG Y, et al. hUCMSC-derived exosomes protect against GVHD-induced Endoplasmic reticulum stress in CD4(+) T cells by targeting the miR-16-5p/ATF6/CHOP axis [J]. Int Immunopharmacol. 2024;135:112315.
20. ASSAF L, EID A A NASSIFJ. Role of AMPK/mTOR, mitochondria, and ROS in the pathogenesis of endometriosis [J]. Life Sci. 2022;306:120805.
21. BAO Z, LI J, CAI J, et al. Plasma-derived exosome miR-10a-5p promotes premature ovarian failure by target BDNF via the TrkB/Akt/mTOR signaling pathway [J]. Int J Biol Macromol. 2024;277(Pt 1):134195.
22. LI Z, ZHANG M. Human umbilical cord mesenchymal stem Cell-Derived exosomes improve ovarian function and proliferation of premature ovarian insufficiency by regulating the Hippo signaling pathway [J]. Front Endocrinol (Lausanne). 2021;12:711902.
23. GAO T, CHEN Y, HU M, et al. MicroRNA-22-3p in human umbilical cord mesenchymal stem cell-secreted exosomes inhibits granulosa cell apoptosis by targeting KLF6 and ATF4-ATF3-CHOP pathway in POF mice [J]. Apoptosis. 2023;28(7–8):997–1011.
24. CHEN Y, ZHAO Y, MIAO C, et al. Quercetin alleviates cyclophosphamide-induced premature ovarian insufficiency in mice by reducing mitochondrial oxidative stress and pyroptosis in granulosa cells [J]. J Ovarian Res. 2022;15(1):138.
25. HU Y Y, ZHONG R H, GUO X J, et al. Jinfeng pills ameliorate premature ovarian insufficiency induced by cyclophosphamide in rats and correlate to modulating IL-17A/IL-6 axis and MEK/ERK signals [J]. J Ethnopharmacol. 2023;307:116242.
26. GUAHMICH NL, WANG MANL. Human theca arises from ovarian stroma and is comprised of three discrete subtypes [J]. Commun Biol. 2023;6(1):7.
27. TAJIMA K, ORISAKA M, YATA H, et al. Role of granulosa and theca cell interactions in ovarian follicular maturation [J]. Microsc Res Tech. 2006;69(6):450–8.
28. VLIEGHE H, LEONEL E C R, ASIABI P, et al. The characterization and therapeutic applications of ovarian theca cells: an update [J]. Life Sci. 2023;317:121479.
29. MIZUSHIMA N. Autophagy in mammalian development and differentiation [J]. Nat Cell Biol. 2010;12(9):823–30.
30. LIN M, HUA R, MA J, et al. Bisphenol A promotes autophagy in ovarian granulosa cells by inducing AMPK/mTOR/ULK1 signalling pathway [J]. Environ Int. 2021;147:106298.
31. YANG Y, TANG X, YAO T, et al. Metformin protects ovarian granulosa cells in chemotherapy-induced premature ovarian failure mice through AMPK/PPAR-gamma/SIRT1 pathway [J]. Sci Rep. 2024;14(1):1447.
32. KIM JY, RHIM W K, YOO Y I, et al. Defined MSC exosome with high yield and purity to improve regenerative activity [J]. J Tissue Eng. 2021;12:20417314211008626.
33. ZHANG S, CHUAH S J, LAI R C, et al. MSC exosomes mediate cartilage repair by enhancing proliferation, attenuating apoptosis and modulating immune reactivity [J]. Biomaterials. 2018;156:16–27.
34. EBRAHIM N, AL SAIHATI H A, ALALI Z, et al. Exploring the molecular mechanisms of MSC-derived exosomes in Alzheimer's disease: autophagy, insulin and the PI3K/Akt/mTOR signaling pathway [J]. Biomed Pharmacother. 2024;176:116836.
35. CAO M, ZHAO Y, CHEN T, et al. Adipose mesenchymal stem cell-derived Exosomal MicroRNAs ameliorate polycystic ovary syndrome by protecting against metabolic disturbances [J]. Biomaterials. 2022;288:121739.
36. XIONG Y, XIONG Y, ZHANG H, et al. hPMSCs-Derived Exosomal miRNA-21 protects against Aging-Related oxidative damage of CD4(+) T cells by targeting the PTEN/PI3K-Nrf2 Axis [J]. Front Immunol. 2021;12:780897.
37. SUN B, MA Y, WANG F, et al. miR-644-5p carried by bone mesenchymal stem cell-derived exosomes targets regulation of p53 to inhibit ovarian granulosa cell apoptosis [J]. Stem Cell Res Ther. 2019;10(1):360.
38. DING C, ZHU L, SHEN H, et al. Exosomal miRNA-17-5p derived from human umbilical cord mesenchymal stem cells improves ovarian function in premature ovarian insufficiency by regulating SIRT7 [J]. Stem Cells. 2020;38(9):1137–48.
39. ZHANG S, ZOU X, FENG X, et al. Exosomes derived from hypoxic mesenchymal stem cell ameliorate premature ovarian insufficiency by reducing mitochondrial oxidative stress [J]. Sci Rep. 2025;15(1):8235.
40. TANG L, YANG Y, YANG M, et al. miR-21-loaded bone marrow mesenchymal stem cell-derived exosomes inhibit pyroptosis by targeting MALT1 to repair chemotherapy-induced premature ovarian insufficiency [J]. Cell Biol Toxicol. 2024;41(1):3.

Publisher's note